HTML ABSTRACT + LINKS

JOURNAL OF APPLIED PHYSICS VOLUME 96, NUMBER 7 1 OCTOBER 2004

Growth of Mn-Bi films on Si(111): Targeting epitaxial MnBi

U. Deffke, G. Ctistis, J. J. Paggel, and P. Fumagalli
Institut für Experimentalphysik, Freie Universität Berlin, 14195 Berlin, Germany

U. Bloeck
Hahn-Meitner-Institut, 14109 Berlin, Germany

M. Giersig
CAESAR, 53175 Bonn, Germany

(Received 25 November 2003; accepted 7 July 2004)

MnBi is of high interest for application as active layer in magneto-optic data storage media for several decades. Here the molecular-beam-epitaxy growth of Mn-Bi films on Si(111) surfaces is investigated under ultrahigh vacuum conditions by means of reflection high-energy electron diffraction, low-energy electron diffraction with spot-profile analysis, Auger-electron spectroscopy, magneto-optic Kerr spectroscopy, and transmission electron microscopy to reveal the microscopic film structure, film composition, and magnetic properties. The film parameters and growth protocols are varied but none of the chosen conditions lead to the formation of MnBi from the two elements. The affinity of Mn to the substrate material Si must be regarded as major reason for the fact that no MnBi forms. © *2004 American Institute of Physics*. [DOI: 10.1063/1.1786377]

Since the 1950s, MnBi has been one of the most intensively discussed materials for application as a magneto-optic data-storage medium.[1–5] In contrast to its favorable magneto-optic properties of a high Kerr rotation in the blue spectral range, which is favorable for high storage density, MnBi shows several temperature dependent problems with respect to its crystalline and magnetic stability.[6–9] In order to overcome these difficulties, a controlled manipulation of structural parameters should be helpful. This, however, needs a controlled growth process. For many decades, various groups have been trying to improve the growth process of MnBi aiming at epitaxial growth but without real success.[5,7,10–12] One of the most successful methods to produce c axis oriented MnBi films is the deposition of one or more double layers of ~18 nm Bi and ~12 nm Mn on a glass or quartz substrate under high-vacuum conditions at room-temperature (RT), followed by an annealing step around T=300 °C.[4] This procedure yields $Mn_{55}Bi_{45}$ films, the best composition with respect to the magneto-optic properties. In most cases, the $(Mn/Bi)_x$ layer structure was covered with SiO_x before annealing.[11,13] The necessity of this protective layer is disputed. Some publications claim that a compound of Mn and Bi is not possible without the cover,[14] whereas in Ref. 4 the authors present MnBi films of good quality without the cover. In the latter case the films, however, very likely have a MnO layer on top, which might have formed unintentionally since the vacuum conditions during growth and annealing were only in the high-vacuum regime.

To gain maximum control of the experiment, we use molecular-beam epitaxy (MBE) under ultrahigh vacuum (UHV) conditions on a Si(111) surface. The capping layer is abandoned, as it disturbs our surface-sensitive sample characterization. The Si(111) surface is chosen as a consequent first step from the amorphous (or polycrystalline) glass or quartz substrates to an ideal lattice-matched substrate. With its threefold symmetry, the Si(111) surface matches the hexagonal symmetry of c axis oriented MnBi. The lattice parameter are $a=4.29$ Å and $c=6.126$ Å for MnBi, and $a=3.84$ Å for the Si(111) plane.

Sample preparation and most of the analytical experiments were performed in a three-chamber UHV-MBE system. During growth, the crystalline structure was monitored with reflection high-energy electron diffraction (RHEED) using a 50 keV electron gun (VTS Createc HP-4). Low-energy electron diffraction with spot-profile analysis (SPA-LEED) was measured with a Leybold electron optic, Auger-electron spectroscopy (AES) by the use of a cylindrical mirror analyzer (Physical Electronics) in the analysis chamber of the vacuum system. The pressure was below 10^{-9} mbar during film growth and below 10^{-10} mbar during analysis. Transmission electron microscopy (TEM) data were taken *ex situ* with a Philips 120 keV CM 12 microscope. Measurements of the magneto-optic Kerr effect (MOKE) were performed in air. MOKE is our most sensitive experimental technique to detect the formation of c-axis oriented MnBi. As none of our samples showed a magnetic signal, no MOKE data will be displayed here.

The samples are of (12×12) mm^2 in size, mounted using tantalum clips on 2 in. molybdenum sample holders which can be heated by a radiation field from the backside. A calibrated quartz microbalance is used to monitor the film thickness. Two different reconstructions of the Si(111) surface served as substrates. Their preparation includes the following steps: Si(111) wafers [both types, n-type doped (phosphorous) and p-type doped (boron)] are first treated chemically with an RCA-clean procedure[15] to obtain a clean protective oxide layer. This oxide is removed thermally in UHV by heating the sample to 1200 °C for 2 min. A cooling procedure leads to the formation of the Si(111)-7×7 surface reconstruction, the first substrate. Exposing this surface to a Bi flux equivalent to about 0.1–1.0 Å/min at 500 °C yields a $\sqrt{3}\times\sqrt{3}$-reconstruction on the Si(111) surface induced by a

0021-8979/2004/96(7)/3972/4/$22.00 © 2004 American Institute of Physics

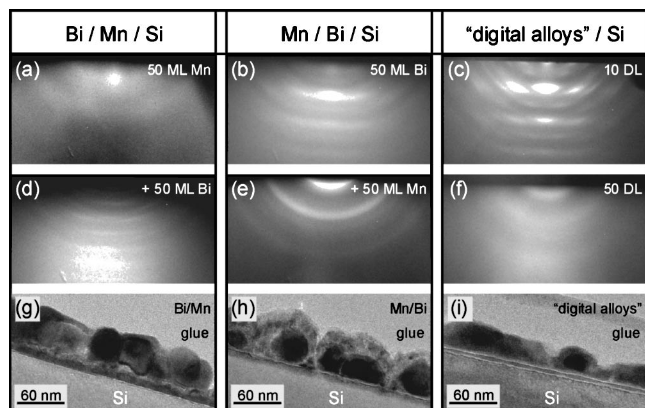

FIG. 1. RHEED [(a)–(f)] and TEM [(g)–(i)] data of Bi/Mn/Si, Mn/Bi/Si, and digital alloys/Si films.

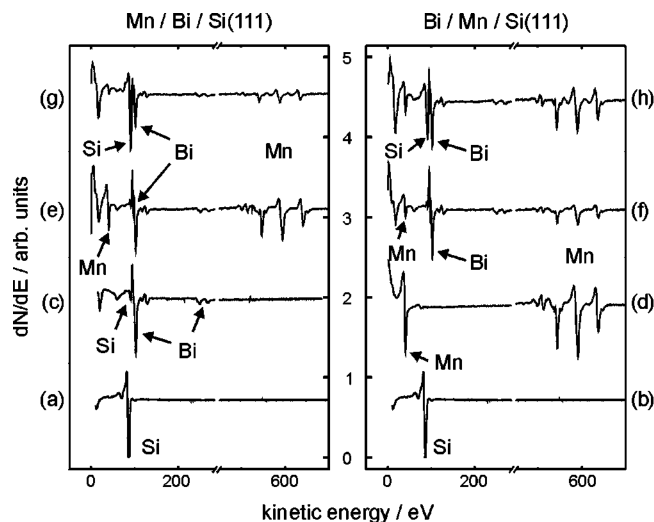

FIG. 2. Two series of Auger spectra: Mn/Bi/Si (left) and Bi/Mn/Si (right). Spectra of the bare 7×7-reconstructed Si substrate [(a),(b)], after the RT deposition of the first [(c), (d)] and second [(e), (f)] component, and after annealing [(g), (h)].

saturation coverage of 1 monolayer (ML) Bi (as judged by AES). This is the second substrate.

Mn was evaporated from a Knudsen cell with rates of ~1 Å/min, Bi was evaporated from a mini electron-beam heated crucible (Oxford Applied Research) with rates of 1.4 Å/min and 3 Å/min dependent on the composition of the film.

The films were prepared in four different ways.

(1) Thick double layers of 50 ML Bi followed by 50 ML Mn (Mn/Bi).

(2) 50 ML of both materials in reverse order (Bi/Mn).

(3) 50 double layers of Bi and Mn, composed as "digital alloys": $50\times$(1 ML Mn/1 ML Bi).

(4) Coevaporation of both materials with fluxes, equivalent to a 1:1-film composition.

All films have a final thickness of ~185 Å, corresponding to 50 ML of each material. (TEM samples are 100 ML thick.) 1 ML equals 7.83×10^{14} atoms/cm^2, the atom density of the Si(111) surface. The nominal thickness of 1 ML Mn as calculated from its RT α-phase structure is thus 0.952 Å. For 1 ML Bi, we calculate a nominal thickness of 2.76 Å per ML from its rhombohedral structure.

All films were grown at RT unless stated otherwise. A postgrowth annealing was conducted at temperatures in the range of 250–350 °C for up to 9 h. For the digital alloys and coevaporated samples, also a growth temperature of 300 °C was used.

Although our study includes the growth of Mn-Bi films on two different Si(111) surfaces most data are presented for the pure Si substrate, as experiments show no significant influence of the substrate termination.

RT deposition of any type of Mn-Bi films does not lead to well ordered crystalline film growth, demonstrated in Fig. 1, showing RHEED patterns of Bi/Mn [(a), (d)], Mn/Bi [(b), (e)] and digital alloy films [(c), (f)]. Samples prepared by coevaporation generate identical RHEED patterns as digital alloys, and thus will not be discussed individually here. We find more or less diffuse ring patterns indicating amorphous or polycrystalline growth. Nevertheless, the RHEED patterns are of characteristic type for the grown material: The Bi growth is characterized by a more textured pattern with intensity maxima along the rings [Figs. 1(b) and 1(d)] and weak and broad horizontal lines. RHEED patterns from the Mn films only consist of a few wide rings [Figs. 1(a) and 1(e)]. Thus, it is difficult to learn anything about the crystalline structure of the Mn and Bi phases. Two important facts are as follows. (i) The reverse film composition of the thick double-layered films can be recognized in the RHEED patterns of Figs. 1(a), 1(d), 1(b), and 1(e). (ii) The digital alloy type of film preparation [(c), (f)] leads to a similar film growth mode as the Mn/Bi-type [(b), (e)]. The same holds for the coevaporated samples. Thus, at RT a monolayerwise material deposition does not lead to a monolayerwise film growth.

TEM images show the influence of the different growth procedures on the sample structures in real space [Figs. 1(g)–1(i)]. These micrographs show ~250 nm wide cross sections of the samples. All films cover the substrate completely. The films consist of two main elements: large, single-crystalline islands of Bi, 30–60 nm in diameter (imaged dark), and a smoother, substrate- or island-covering layer of Mn (imaged bright). This material assignment corresponds well with the RHEED observations. It is confirmed by analysis of the crystalline structure in high-resolution data identifying α-Mn and Bi crystallites in these films (not shown here), by EDAX-measurements (energy dispersive analysis of x-rays, also not shown), as well as by the fact, that heavy elements absorb more electrons and are thus displayed dark in TEM.

AES data are consistent with this picture. Figure 2 shows two series of Auger spectra: on the left, a Mn/Bi/Si film and, on the right, a Bi/Mn/Si film. Each series starts with a spectrum of the bare Si(111)-7×7 substrate at the bottom [(a), (b)], followed by spectra of the RT-grown 50 ML of the first material—Bi (c) and Mn (d)—covered with the second

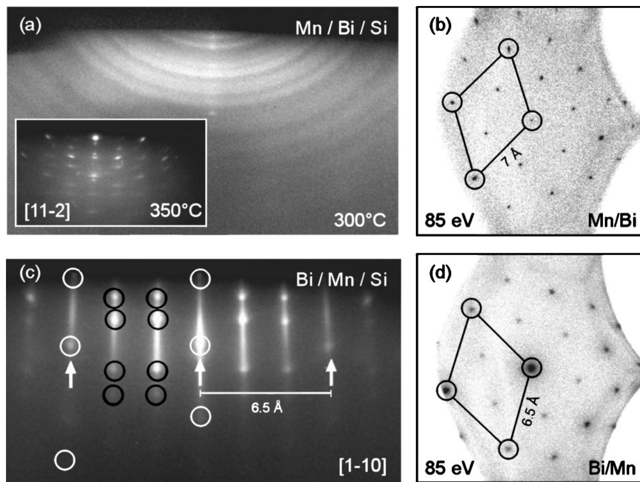

FIG. 3. Diffraction patterns of the annealed films. (a) RHEED pattern of the Bi/Mn/Si film after 9 h annealing at 300 °C. (b) LEED pattern of the same surface. Inset of (a): pattern of a digital alloy film after 9 h annealing at 350 °C. (c) RHEED and (d) LEED pattern of the annealed Mn/Bi/Si film. (Unit cell indicated by diamond.)

material—Mn (e) and Bi (f)—and ends with the spectrum of the annealed film—9 h at 300 °C (g) and 1 h at 300 °C +15 min at 350 °C (h).

The material deposited first covers the substrate: only very little traces of Si—if at all—can be found in the spectra (c) and (d). They vanish completely after deposition of the second material. However, the characteristic Auger transitions of the film grown first remain visible in both cases, showing that either the on-top material does not cover the underlying film completely or that some intermixing of both materials takes place. According to the TEM data, the latter seems to take place. The intensity ratio is just as expected from the deposition sequence.

To summarize the growth process at RT, we find closed films with both materials growing in separate phases, irrespective of the deposition method. The films are rough and do not exhibit good crystalline quality.

This changes after annealing the samples. The annealing experiments were carried out in two different ways: series of short-time anneals with increasing temperature (10 min at 100 °C, followed by 10 min at 200 °C and 30 min at 300 °C) to study the onset of structural changes, and long-time annealing (9 h) at different temperatures (250 °C, 300 °C, 350 °C).

Annealing the RT-grown films leads to structural changes indicated by modifications in the RHEED pattern. For samples with comparable RT structure (Mn/Bi, digital alloys, coevaporated), a similar stuctural evolution is observed. Around 100 °C, the polycrystalline texture vanishes and the diffraction pattern is characterized by diffuse intensity only. At temperatures higher than 250 °C, crystalline ordering takes place leading to the formation of a characteristic polycrystalline ring pattern after 30 min at 300 °C [Fig. 3(a)]. For longer annealing times of up to 9 h (at 300 °C), the structure remains unchanged but the pattern gains intensity. Increasing the temperature to 350 °C yields a complex pattern of bulk spots as a superposition to the ring pattern [Fig. 3(a) inset]. The ring pattern is unique. The same holds for the bulk spots. Nevertheless, we attribute the ring pattern to a Bi phase, as will become clear during further discussion.

The polycrystalline RHEED pattern indicates a rough film. Therefore it is surprising to observe LEED patterns of high quality from the same surface [Fig. 3(b)]. All types of samples discussed so far (Mn/Bi/Si, digital alloys, coevaporated) show the same LEED pattern originating from ~15 nm large well-ordered crystalline domains as revealed from the full width at half maximum via spot-profile analysis. The symmetry is of $\sqrt{3}\times\sqrt{3}$ type as deduced from the spot-intensity distribution. The lattice constant is 7 Å. It cannot be assigned to the MnBi or to the Bi or Mn lattices. LEED interpretation is aided by our investigations of the growth process of Mn on the Si(111)-7×7 and Si(111)-$\sqrt{3}\times\sqrt{3}$:Bi surfaces,[16] identifying this phase as Mn_5Si_3.

Annealing the Bi/Mn/Si sample at 300 °C for up to 1 h leads to the formation of a streaky RHEED pattern. Its quality can be increased by further annealing to 350 °C for 15 min yielding the diffraction patterns of Figs. 3(c) and 3(d). The streaky RHEED pattern (c) indicates high surface quality and shows characteristic features already known from the growth of Mn on Si(111) [compare Fig. 1 (d) of Ref. 16]: MnSi forms.

This interpretation is confirmed by AES [Figs. 2(g) and 2(h)]. The films grow as closed layers on the substrate at RT. No sign of Si is visible without annealing [Figs. 2(e) and 2(f)]. Annealing leads to a dramatic change. With increasing annealing time and temperature, a Si peak is growing and becomes a significant part of the spectrum. Figure 2(g) shows the situation after 9 h annealing at 300 °C when a steady state is reached. When judged from the AES spectra alone, the appearance of Si might be explained with a partially uncovered substrate surface due to possible island formation. This explanation is not compatible with the diffraction and TEM data showing flat and well closed films over wide areas. We thus have to conclude, that Si is detected from the film surface, where it builds a well-structured overlayer or a Mn silicide, respectively (compare to Ref. 16).

Diffraction and AES experiments on high temperature digital alloy growth on the two different Si(111) substrates have shown that there is crystalline order in the film surface only if it contains Si. Si diffusion to the film surface is suppressed by depositing 50 DL digital alloys at 200 °C substrate temperature on the Bi reconstructed Si surface [Fig. 4(a)]. No LEED pattern can be measured from this sample. In contrast, deposition on the pure Si substrate under the same conditions yields Si in the Auger spectrum [Fig. 4(b)] and a $\sqrt{3}\times\sqrt{3}$ LEED pattern (not shown here).

The composition of our samples—Bi islands and flat Mn films even at RT—is in contrast to the one observed by Rüdiger *et al.*,[4] who claim the exactly opposite behavior of both materials during RT deposition on glass substrates: whereas Mn builds islands, Bi grows as a flat crystalline oriented film on top of the substrate as well as on top of Mn. This difference might be due to the choice of the substrate.

In conclusion, a variety of attempts has been made to grow *c* axis texured MnBi films on Si(111) surfaces—none was successful as no magnetic signal was obtained from any of the films. Instead of forming MnBi, both materials survive

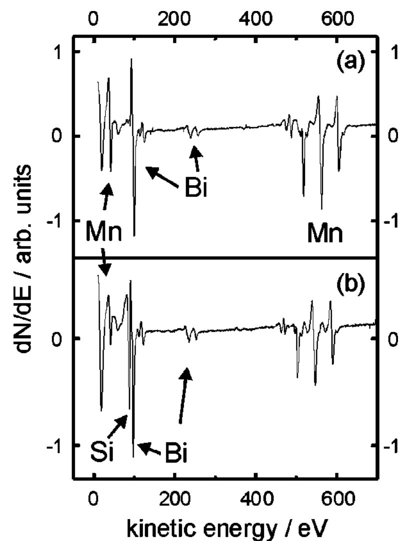

FIG. 4. AES spectra of 50 DL digital alloy films deposited at 200 °C (a) on a Si(111)-$\sqrt{3}\times\sqrt{3}$:Bi surface and (b) on a Si(111)-7×7 surface. The striking difference is the Si peak at 91 eV which is visible in (b) but not in (a).

in separate phases even during coevaporation and after long annealing procedures or deposition at higher temperatures. The Si substrate plays a key role in this process: Mn tends to form silicides of probably a few ten ML in thickness. This silicide builds flat films on the substrate with a high-quality crystalline order. Bi in contrast diffuses to the top of the film.

ACKNOWLEDGMENT

We acknowledge the financial support of the Deutsche Forschungsgemeinschaft through SFB 290.

[1]H. J. Williams, R. C. Sherwood, F. G. Foster, and E. M. Kelley, J. Appl. Phys. **28**, 1181 (1957).
[2]B. W. Roberts, Phys. Rev. **104**, 607 (1956).
[3]Di Chen, Gary N. Otto, and Francis M. Schmit, IEEE Trans. Magn. **MAG-9**, 66 (1973).
[4]U. Rüdiger, H. Berndt, A. Schirmeisen, P. Fumagalli, and G. Güntherodt, J. Appl. Phys. **78**, 5391 (1995).
[5]J. Schoenes, K.-U. Harder, D. Menzel, and T. Widmer, J. Magn. Soc. Jpn. **23**, 95 (1999).
[6]R. R. Heikes, Phys. Rev. **99**, 446 (1955).
[7]X. Guo, X. Chen, Z. Altounian, and J. O. Ström-Olsen, Phys. Rev. B **46**, 14578 (1992).
[8]Di Chen, J. Appl. Phys. **42**, 3625 (1971).
[9]A. F. Andresen, W. Hälg, P. Fischer, and E. Stoll, Acta Chem. Scand. **21**, 1543 (1997).
[10]X. Guo, A. Zaluska, Z. Altounian, and J. O. Ström-Olsen, J. Mater. Res. **5**, 2646 (1990).
[11]M. Nakada and M. Okada, IEEE Trans. Magn. **30**, 4431 (1994).
[12]R. Hayashi, K. Terayama, T. Ishibashi, and K. Sato, J. Magn. Soc. Jpn. **23**, 99 (1999).
[13]G.-Q. Di, S. Oikawa, S. Tsundashima, and S. Uchiyama, Jpn. J. Appl. Phys. **33-2**, L783 (1994).
[14]K.-U. Harder, D. Menzel, T. Widmer, and J. Schoenes, J. Appl. Phys. **84**, 3625 (1998).
[15]W. Kern, *Handbook of Semiconductor Wafer Cleaning Technology* (Noyes Publication, Norwich, NY, 1993).
[16]G. Ctistis, U. Deffke, K. Schwinge, J. J. Paggel, and P. Fumagalli, (unpublished).